

# A Foldable Stereo Vision Unit for Single Port Access Laparoscopy

Kai Xu\*, Member, IEEE, Jiangran Zhao, Student Member, IEEE, and Zhengchen Dai

**Abstract**—SPAL (Single Port Access Laparoscopy) could lead to improved surgical outcomes but demands functional and effective next-generation surgical tools. Various manual tools and robotic assistant systems have been developed in response to the unmet needs of SPAL. This paper presents the concept, design considerations and experimental characterizations of a foldable stereo vision unit with integrated illumination. The vision unit can be inserted into the abdomen through a  $\text{\O}12\text{mm}$  trocar in a cylindrical laparoscope form. It can then unfold itself into a working configuration, providing 3D visualization of the surgical site as well as a remaining access port for manipulation arms or surgical tools. Given its standalone features, the vision unit could either be used for SPAL in a robotic assistant system or be applied in a surgical setting with standard manual tools.

## I. INTRODUCTION

SPAL (Single Port Access Laparoscopy) uses one skin incision (usually the umbilicus) for surgical interventions [1]. Compared with traditional multi-port laparoscopic MIS (Minimally Invasive Surgery), SPAL could further improve surgical outcomes in terms of complication rates, postoperative pain, hospitalization time and cosmesis in a similar clinical setting [2]. Even more recently introduced, NOTES (Natural Orifice Translumenal Endoscopic Surgery), which only uses a patient's natural orifices (such as vagina, GI track, etc) for scar-less surgeries [3], could be more tempting than SPAL. However, even assisted by the state-of-the-art tool instrumentation [4] and robotics technology [5-11], NOTES is still quite far from massive clinical trials.

Equipped with newly developed SPAL tools (e.g. the TriPort from Advanced Surgical Concepts, the SILS port from Covidien, the RealHand tools from Novare Surgical Systems, and the Cambridge Endo instruments), Surgeons have found SPAL a viable option over traditional laparoscopy [12, 13]. Besides the development of the manual tools, several robotic assistant systems were also built in order to ease the challenging hand-eye coordination while manipulating the curved cross-posed SPAL tools. These robotic systems include the stackable four-bar linkage for SPAL [14], the  $\text{\O}23\text{mm}$ -port SPAL robot [15], the  $\text{\O}30\text{mm}$ -port SPAL robot [16], the SPAL toolset (a  $\text{\O}35\text{mm}$  port for a scope, two curved tools and one channel) for the da Vinci surgical robot [17], and the  $\text{\O}15\text{mm}$ -port IREP (Insertable Robotic Effector

Platform) robot [18, 19].

Robotic assistants are intuitive and easy to operate but they are often involved with regulatory hurdles and high costs. On the other hand, manual SPAL tools are cheaper and prevail relatively faster but surgeons need to go through substantial trainings to be skilled. This paper hence presents the design of a foldable stereo vision unit, which can be integrated into a robotic assistant system for SPAL and/or be applied as a handheld tool for manual SPAL. The vision unit integrated with illumination is shown in Fig. 1. It has a cylindrical laparoscope form with a diameter of 12mm. In this form it can be inserted into abdomen through a standard trocar. The vision unit can then unfold itself into a working configuration, providing a remaining access port and 3D visualization of the surgical site. Robotic manipulation arms or manual tools can then be deployed via this remaining port.

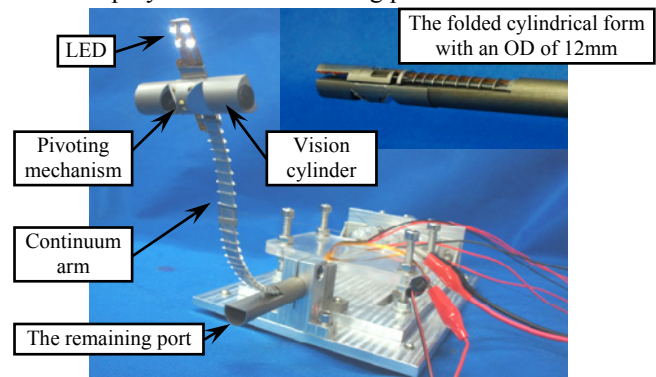


Fig. 1. The foldable stereo vision unit for SPAL

A similar work can be found in [20], where a magnetically anchored  $\text{\O}22\text{mm}$  3D vision unit was developed for SPAL. Several distinctive features are presented by this paper, which forms the main contributions of this work. The distinctive features include i) the use of a continuum arm, and ii) a camera pivoting mechanism. The continuum arm allows easy positioning and overarching of the vision unit to avoid collisions with the inserted tools. The camera pivoting mechanism enables the deployment of two  $\text{\O}7.8\text{mm}$  camera heads through a  $\text{\O}12\text{mm}$  trocar.

The paper is organized as follows. Section II presents the design goals and Section III presents considerations and detailed descriptions of the vision unit. Since the major contribution of this paper is the mechanical design of this stereo vision unit, the experimental characterization as in Section IV follows existing conventional methods. The conclusions are followed in Section V.

## II. DESIGN GOALS AND OVERVIEW

Motivated by the increasing demands for SPAL, this paper

Manuscript received Sept 15<sup>th</sup>, 2013. This work is supported in part by the National Natural Science Foundation of China (Grant No. 51005146 and Grant No. 51375295) and in part by the Shanghai Pujiang Scholar Program (Grant No. 11PJ1405600).

The authors are with the RII Lab (Lab of Robotics Innovation and Intervention), UM-SJTU Joint Institute, Shanghai Jiao Tong University, Shanghai, 200240, China (asterisk indicates the corresponding author, phone: 86-21-34207220; fax: 86-21-34206525; emails: k.xu@sjtu.edu.cn, zjr318@sjtu.edu.cn, and zhengchen.dai@sjtu.edu.cn).

proposes to design a foldable stereo vision unit applicable both in a robotic surgical system and as a handheld device for manual operations.

When the vision unit is in its folded configuration, it can be inserted into abdomen through a skin incision (usually the umbilicus). After insertion, the vision unit can unfold itself into a working configuration, providing a remaining access port and 3D visualization of the surgical site.

The vision unit could be used as a handheld device as shown in Fig. 2(a). The access port shall be big enough to pass a standard ablation tool (e.g. the 5mm Ethicon Harmonic scalpel) and/or for water/gas sources. Two needle-like laparoscopic tools (e.g. the Stryker MiniLap tools or the Karl Storz Mini-Laparoscopy tools) can be inserted into the abdomen for tissue manipulations. The vision unit could also be applied in a robotic surgical system as shown in Fig. 2(b). Two robotic manipulators with grippers or cautery tips could be inserted from the access port to perform surgical tasks.

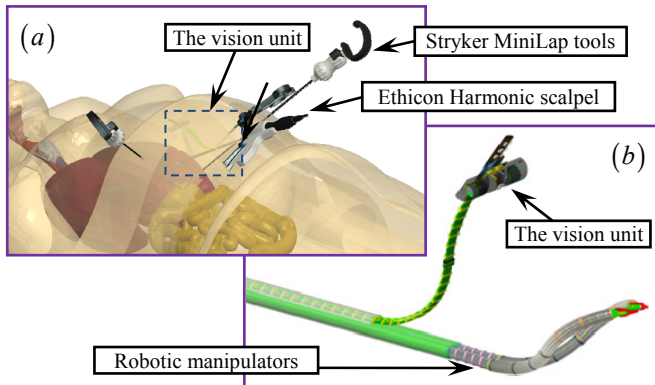


Fig. 2. Two possible application concepts for this vision unit: (a) as a handheld device for manual SPAL, or (b) in a robotic surgical system

Taking into consideration the applicable scenarios of this vision unit, the prototype is shown in Fig. 1. Distinct features of this design can be highlighted as follows.

- The vision unit only has an outer diameter of 12mm in its folded cylindrical form. This is inspired by the 12mm endoscopic robot in which the access port is big enough for two 5-DoF continuum manipulators [10, 11].
- The camera pivoting mechanism enables the deployment of two  $\text{\O}7.8\text{mm}$  camera heads one by one through a  $\text{\O}12\text{mm}$  trocar. Using two relatively big camera heads could lead to better image quality.
- The optimal imaging distance from the objects to the vision unit shall be between 100mm to 150mm.
- The continuum arm for orienting and positioning of the vision unit has three DoFs (Degrees of Freedom). The two segments could be bent independently and the proximal segment can be extended from the arm entrance port.
- LEDs are integrated for illumination.

Section III presents the design considerations and the components descriptions, including the selection and arrangement of the camera heads, the design of the camera pivoting mechanism, dimension synthesis of the continuum arm, etc. Experimental characterization of this vision unit will be presented in Section IV.

### III. CONSIDERATIONS AND DESCRIPTIONS

This stereo vision unit mainly consists of the vision cylinder with two camera heads, the camera pivoting mechanism, the continuum arm and the LED illumination. These components will be described in detail.

#### A. Camera selection and arrangement

Camera selection is critical for a vision unit. After carefully checking the available products of the major suppliers of miniature camera heads, MO-B3506 from the MISUMI Electronics Corp is picked. This camera head has an outer diameter of 7.8mm and a length of 7.5mm as shown in Fig. 3(c). The resolution is  $640 \times 480$  with an S/N (signal over noise) ratio of 50dB and a minimally required illumination of 0.1 Lux. Although there are camera heads at smaller sizes, they either have a lower resolution, a poorer S/N ratio, or demand higher illumination.

The design goal is to design a stereo vision unit compact enough to pass through a  $\text{\O}12\text{mm}$  trocar. Due to the 7.8mm diameter of the camera head, a serial arrangement of the two camera heads had to be used. While putting the camera head axially with the vision cylinder, a mirror is used to reflect the images. Using a mirror is equivalent to orienting the camera towards a radial direction.

As shown in Fig. 3(a), a back-to-back arrangement was firstly tested. This arrangement generates a baseline distance of 46mm between the two equivalent cameras. However when objects are at the desired viewing distances of between 100mm to 150mm, this is similar to putting objects too close to human eyes. The stereo images from the two camera heads look unnatural and don't trigger a 3D perception.

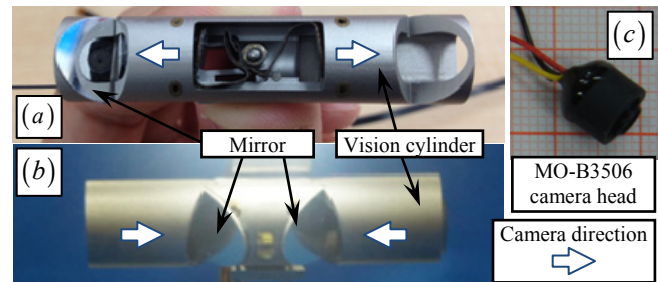


Fig. 3. Camera arrangement of the vision cylinder: (a) the back-to-back arrangement and (b) the face-to-face arrangement

Hence a face-to-face arrangement is then tested as shown in Fig. 3(b) with a more detailed diagram shown in Fig. 4. The distance between the two cameras is 20mm and the distance between the mirror centers is 1mm. If the angle between the two mirrors is  $90^\circ$ , the axes of the two equivalent camera heads are parallel. By adjusting the angle  $\gamma_1$  between the two mirrors, the angle  $\gamma_2$  between the axes of the two equivalent camera heads can be changed according to the geometrical relation in Eq. (1). A series of experiments were carried out to determine what  $\gamma_2$  value is the best to trigger 3D perception for human. As shown in Fig. 4(c), a few plastic frames made from 3D printing were used to hold the cameras in equivalent positions for different  $\gamma_2$  values. The anaglyph views were

presented to 5 human subjects for them to vote which one looked the most natural. The one with  $\gamma_1 = 92^\circ$  was chosen.

$$\gamma_2 = 2\gamma_1 - 180^\circ \quad (1)$$

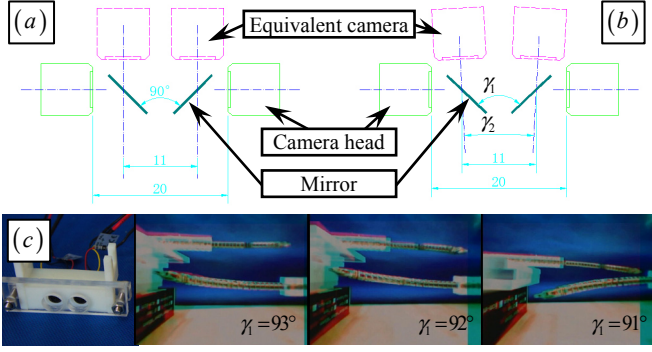


Fig. 4. Determine the camera arrangement: (a) parallel equivalent camera axes, (b) crossed equivalent camera axes, and (c) experiments to decide  $\gamma_1$

### B. Camera pivoting mechanism

Due to the face-to-face serial arrangement of the two camera heads, a pivoting mechanism is needed to rotate the vision cylinder for  $90^\circ$  to generate normal stereo images.

As shown in Fig. 5, the vision cylinder will be driven to rotate about the pivoting screw to transform the vision unit from the cylindrical form into the working configuration.

The actuation block can be driven to move back and forth along the guiding pin in the slot. Enveloping shape of the actuation block is trimmed to guarantee that everything is within the  $\varnothing 12\text{mm}$  cylindrical shape when the vision unit is fully folded. The actuation block is driven by a  $\varnothing 0.4\text{mm}$  actuation rod made from NiTi (nickel-titanium alloy) in a push-pull mode. The driving pin is attached to the vision cylinder and it can slide inside a slot of the actuation block. When the actuation block is actuated by the actuation rod to move back and forth, it pushes the driving pin to rotate the vision cylinder from the pose as in Fig. 5(a) to Fig. 5(c).

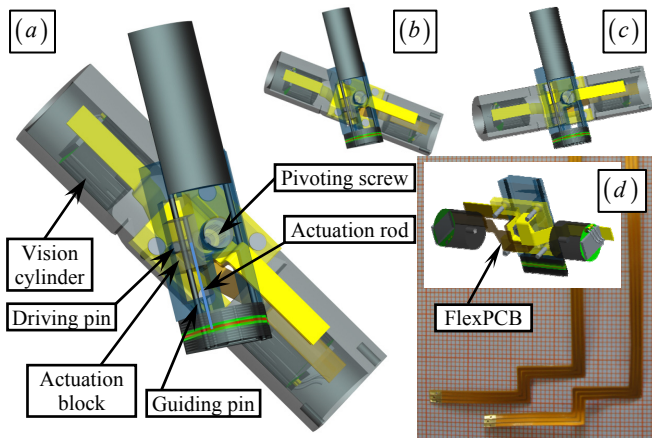


Fig. 5. Camera pivoting mechanism: (a) ~ (c) unfolding poses and (d) the shape and arrangement of the flexible PCB strips

Besides realizing the desired unfolding motion of the vision cylinder, attention was also paid to the wiring of the two camera heads. Flexible PCB strips were used to replace the cameras' original wires in order to make sure they will not get tangled. As shown in Fig. 5(d), the flexible PCB strips

were carefully routed and patterned to allow the rotation of the vision cylinder.

### C. Structure and dimensions of the continuum arm

Referring to Fig. 1, the continuum arm is used to position and orient the vision unit. As shown in Fig. 6, the continuum arm consists of a super-elastic NiTi strip, a fixation ring, spacers and actuation rods.

A fixation ring is rigidly attached to the NiTi strip in the middle of the strip. The portion of the NiTi strip from the fixation ring to the arm entrance port is referred to as segment #1. The actuation rod is attached to the fixation ring and can slide in the holes of the spacers. Pulling of the actuation rod would bend the segment upwards.

The portion of the NiTi strip between the vision unit and segment #1 is referred to as segment #2. Another actuation rod is attached to the vision unit and can slide in the holes of the spacers. Pushing this actuation rod, which is routed through segment #1, would bend segment #2 downwards.

Hence there are 3 DoFs for the continuum arm: 2 DoFs for bending and 1 DoF for the translational feed of segment #1.

Bent shapes of the segments #1 and #2 are assumed to be circular arcs according to the previous studies [21-23]. This assumption will be verified by the experiments in Section IV.B. Following this assumption, a dimension synthesis could be performed to determine the desired lengths of the segments. The desired viewing distance is 100mm to 150mm from the arm entrance as shown in Fig. 7. Segment #1 is also assumed to undergo a  $90^\circ$  bending. Then the following geometrical relations can be derived.

$$\overline{OC} = \frac{2L_1}{\pi} + \frac{L_2}{\vartheta} (1 - \cos \vartheta) \quad (2)$$

$$\overline{BC} = \frac{2L_1}{\pi} + \frac{L_2}{\vartheta} \sin \vartheta \quad (3)$$

$$\overline{CD} = \frac{\overline{BC}}{\tan \vartheta} = \frac{2L_1 \cos \vartheta}{\pi \sin \vartheta} + \frac{L_2 \cos \vartheta}{\vartheta} \quad (4)$$

$$\overline{OD} = \overline{OC} + \overline{CD} = \frac{2L_1}{\pi} \left( 1 + \frac{\cos \vartheta}{\sin \vartheta} \right) + \frac{L_2}{\vartheta} \quad (5)$$

If the bending range of segment #2 is from  $0^\circ$  to  $90^\circ$ , it is desired for the viewing direction to point towards the center of the viewing range when  $\vartheta = 45^\circ$ . Then Eq. (5) gives:

$$\overline{OD} = \frac{4}{\pi} (L_1 + L_2) \rightarrow 125\text{mm} \quad (6)$$

There are many combinations of  $L_1$  and  $L_2$  which satisfy Eq. (6).  $L_1 = 60\text{mm}$  and  $L_2 = 40\text{mm}$  are finally decided for this viewing configuration. Since  $L_1 = 60\text{mm}$ , the travel of the translational DoF of the continuum arm shall be big enough to allow this.

### D. Integrated illumination

Making use of all the available space, eight LEDs were originally planned for the illumination as shown in Fig. 8(a). Flexible PCBs were planned to wire the LEDs as in Fig. 8(d).

The two LEDs at Area #2 were not used due to the difficulty of fixing them in position under the disturbances

from the cameras' flexible PCB strips. The arrangement of the cameras' PCB strips is shown in Fig. 5(d).

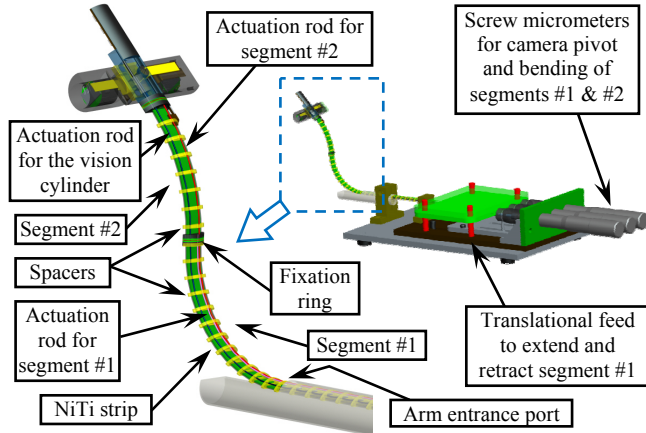


Fig. 6. Structure of the continuum arm

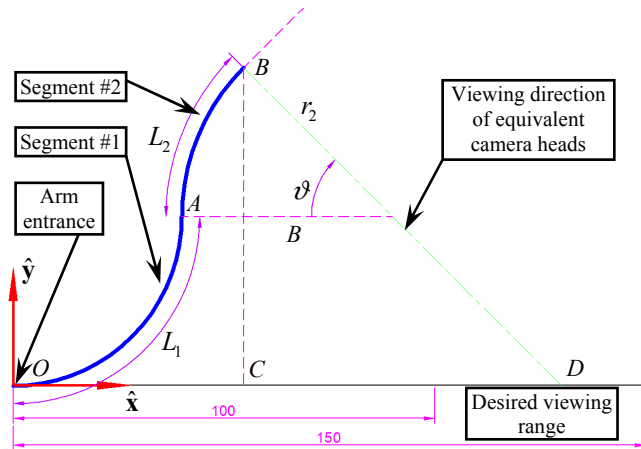


Fig. 7. Dimension synthesis of the continuum arm

Temperature rise is always a concern when LEDs are used for illumination. Two strips were prepared and tested for the potential heating problem. Referring to Fig. 8(a) and (d), six LEDs and four LEDs are soldered to the PCB strip respectively. Temperatures of the LEDs were measured when the LEDs were powered at different voltages in open air under room temperature. The testing results are listed in Table I.

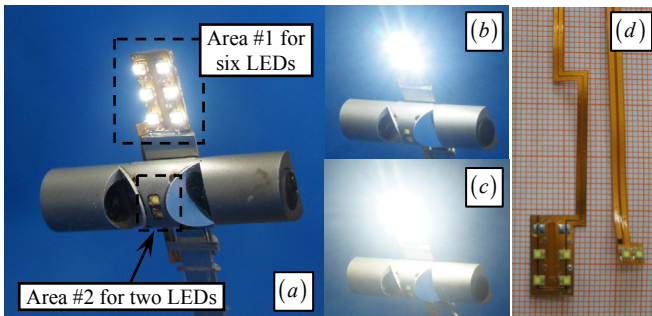


Fig. 8. LED arrangement and illumination brightness with LEDs powered at (a) 2.50v, (b) 2.60v and (c) 2.70v; (d) Flexible PCBs for LEDs

The LED's rated voltage is 2.95 volts. It can be seen from the testing results that using the LEDs at 2.95 volts will cause heating problems no matter whether six or four LEDs are used. The LEDs have to be used at a lower voltage, such as 2.70 volts. It was then decided that six LEDs would be used, as in Fig. 8(a). The maximal supply voltage is 2.70 volts.

Experimental results in Section IV.D would present a qualitative sense whether these LEDs are bright enough.

TABLE I  
LED HEATING TESTS

LED Qty	Voltage (V)	Time (min)	Temperature (°C)
6	2.95	7	126
		20	105
		30	96
	2.70	2	38
		10	36
		30	33
4	2.95	5	72
		15	99
		30	72

#### IV. EXPERIMENTAL CHARACTERIZATION

After the vision unit is fabricated and assembled, a series of experiments were performed to characterize the features of this foldable stereo vision unit.

##### A. Deployment

This foldable vision unit shall be inserted into abdomen in a cylindrical form. Then it unfolds itself to provide visualization. This deployment process shall be verified first.

The deployment is shown in Fig. 9: (a) the vision unit started the process from a cylindrical form whose diameter is 12 mm; (b) then the continuum arm was extended from the entrance to allow enough length of segment #1; (c) segment #1 was bent upwards by pulling one NiTi actuation rod; (d) segment #2 was then bent downwards by pushing the other actuation rod; the camera cylinder was also actuated to rotate about the pivot point; (e) when the segments were bent to the desired shapes, LEDs were powered on and stereo visual feeds were streamed.

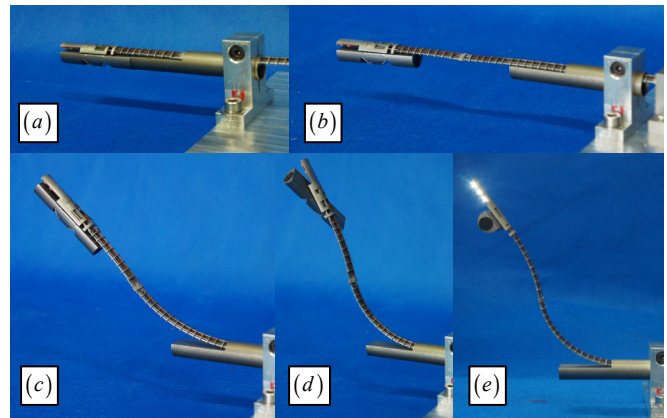


Fig. 9. Deployment of the foldable vision unit

##### B. Bending shape identification

The dimension determination of the continuum arm in Section III.C is based on an assumption that both segments will be bent into circular shapes. Shape identification experiments were hence carried out to verify this assumption.

The experimental setup is shown in Fig. 10. An optical tracker (Micron Tracker SX60, Claron Technology Inc.) with a pointing tool was used. The pointing tool was pointed at various points along the continuum arm. The tracker recognized the markers of the pointing tool and directly

provided coordinates of the tool's tip.

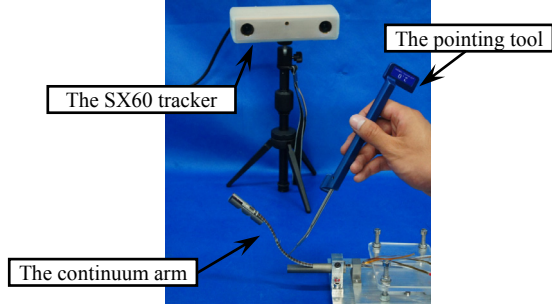


Fig. 10. The experiments for shape identification of the continuum arm

The coordinates of the points along the continuum arm under various poses were recorded, transformed to the frame  $\{\hat{x}, \hat{y}\}$  as defined in Fig. 7, and plotted in Fig. 11. A circular arc connected with a straight line segment was used to approximate two poses in Fig. 11, when segment #2 was not bent. Then two connected circular arcs are used to approximate the other two poses in Fig. 11. From the experimental results, it can be seen that the actual shapes of the continuum arms can be well approximated by two connecting circular arcs.

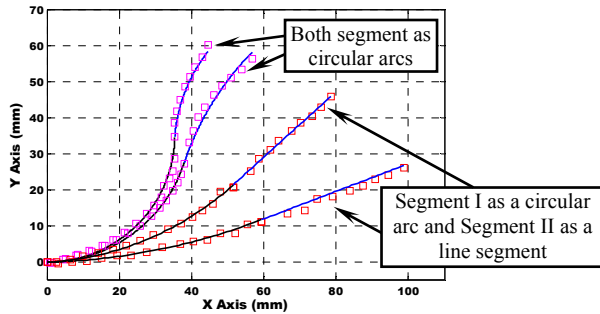


Fig. 11. Shape identification of the continuum arm

### C. Camera calibration and 3D reconstruction

In order to use the stereo vision unit for surgical tool tracking and 3D reconstruction, the camera heads shall be calibrated. The implemented calibration process used the Camera Calibration Toolbox for Matlab<sup>®</sup> developed by Jean-Yves Bouguet using existing algorithms [24, 25]. As shown in Fig. 12(a), a series of pictures were taken of a calibration board with known grid sizes. The corners were extracted and the detection was iterated to obtain the distortion correction coefficients. The distortion can be visualized as in Fig. 12(b). The calibration was repeated for both cameras. The focal lengths, the principal points, the skew coefficient and the distortion coefficients were all obtained. The position and orientation of the right camera with respect to the left camera were also calibrated.

Then the stereo vision unit was tested for 3D reconstruction. The scene is shown in Fig. 13(a). Three blocks were put on a white background. Three extractable cross markers were printed on the background so that a local frame  $\{\hat{x}_i, \hat{y}_i\}$  can be easily defined. Correspondences of the blocks' corners were manually established. The position errors of these points are all between 0.5 mm to 1.2 mm.

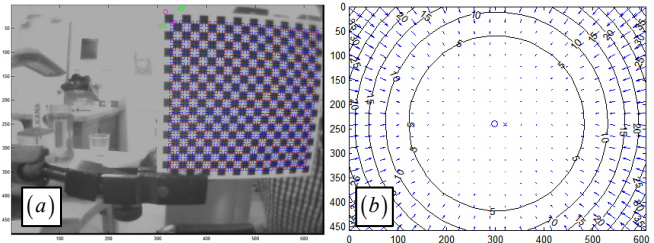


Fig. 12. Camera calibration: (a) pictures taken of a calibration board and (b) visualization of the distortion

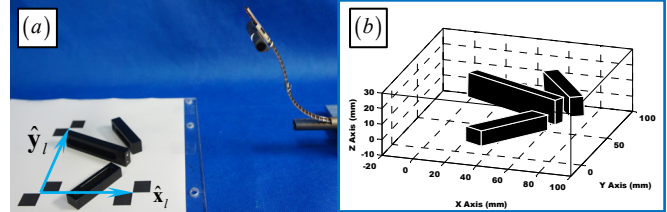


Fig. 13. 3D construction using the calibrated stereo vision unit: (a) the original and (b) the reconstructed scenes

### D. Ex-vivo trial of the vision unit

The stereo vision was also tested in an ex-vivo trial. As shown in Fig. 14(a), a box was used to mimic an abdomen under pneumoperitoneum and the vision unit was deployed. Using the six LEDs powered at 2.7 volts, the scene was successfully visualized. The assembled anaglyph view is shown in Fig. 14(b).



Fig. 14. Ex-vivo trials: (a) the setup and (b) the assembled anaglyph view

## V. CONCLUSIONS AND FUTURE WORK

This paper presents the concept, design considerations and experimental characterizations of a foldable stereo vision unit with integrated illumination. It is possible to use this vision unit either in a robotic assistant system for SPAL or in a surgical setting using manual tools.

The vision unit features a foldable design. It can be inserted into abdomen through a  $\varnothing 12\text{mm}$  trocar in a cylindrical form. Then it can unfold itself into a working configuration, providing 3D visualization of the surgical site as well as a remaining access port for robotic arms or surgical tools.

A series of experiments demonstrated its deployability, identified the shapes of the continuum arm, reconstructed a 3D scene with satisfactory accuracy and visualized a mockup surgical site using its integrated illumination.

The future work will mainly focus on improving the packaging of the current prototype in order to improve the reliability, sterilizability, etc.

## REFERENCES

- [1] G. Navarra, E. Pozza, S. Occhionorelli, P. Carcoforo, and I. Donini, "One-Wound Laparoscopic Cholecystectomy," *British Journal of Surgery*, vol. 84, No.5, p. 695, 1997.
- [2] E. R. Podolsky, L. St. John-Dillon, S. A. King, and P. G. Curcillo II, "Reduced Port Surgery: An Economical, Ecological, Educational, and Efficient Approach to Development of Single Port Access Surgery," *Surgical Technology International*, No.20, pp. 41-46, Oct 2010.
- [3] A. N. Kalloo, V. K. Singh, S. B. Jagannath, H. Niiyama, S. L. Hill, C. A. Vaughn, C. A. Magee, and S. V. Kantsevov, "Flexible Transgastric Peritoneoscopy: a Novel Approach to Diagnostic and Therapeutic Interventions in the Peritoneal Cavity," *Gastrointestinal Endoscopy*, vol. 60, No.1, pp. 114-117, July 2004.
- [4] B. Hu, S. Chung, L. C. L. Sun, K. Kawashima, T. Yamamoto, P. B. Cotton, C. J. Gostout, R. H. Hawes, A. N. Kalloo, S. V. Kantsevov, and P. J. Pasricha, "Eagle Claw II: a Novel Endosuture Device that Uses a Curved Needle for Major Arterial Bleeding: a Bench Study," *Gastrointestinal Endoscopy*, vol. 62, No.2, pp. 266-270, 2005.
- [5] D. J. Abbott, C. Becke, R. I. Rothstein, and W. J. Peine, "Design of an Endoluminal NOTES Robotic System," in *IEEE/RSJ International Conference on Intelligent Robots and Systems (IROS)*, San Diego, CA, USA, 2007, pp. 410 - 416.
- [6] S. J. Phee, S. C. Low, Z. L. Sun, K. Y. Ho, W. M. Huang, and Z. M. Thant, "Robotic System for No-Scar Gastrointestinal Surgery," *The International Journal of Medical Robotics and Computer Assisted Surgery*, vol. 4, No.1, pp. 15-22, March 2008.
- [7] A. C. Lehman, J. Dumpert, N. A. Wood, L. Redden, A. Q. Visty, S. Farritor, B. Varnell, and D. Oleynikov, "Natural Orifice Cholecystectomy using a Miniature Robot," *Surgical Endoscopy*, vol. 23, No.2, pp. 260-266, Feb 2009.
- [8] G. Tortora, A. Dimitracopoulos, P. Valdastrì, A. Menciassi, and P. Dario, "Design of Miniature Modular in vivo Robots for Dedicated Tasks in Minimally Invasive Surgery," in *IEEE/ASME International Conference on Advanced Intelligent Mechatronics (AIM)*, Budapest, Hungary, 2011, pp. 327-332.
- [9] K. Xu, J. Zhao, J. Geiger, A. J. Shih, and M. Zheng, "Design of an Endoscopic Stitching Device for Surgical Obesity Treatment Using a N.O.T.E.S Approach," in *IEEE/RSJ International Conference on Intelligent Robots and Systems (IROS)*, San Francisco, CA, USA, 2011, pp. 961-966.
- [10] K. Xu, J. Zhao, and A. J. Shih, "Development of an Endoscopic Continuum Robot to Enable Transgastric Surgical Obesity Treatment," in *International Conference on Intelligent Robotics and Applications (ICIRA)* Montreal, Quebec, Canada, 2012, pp. 589-600.
- [11] J. Zhao, X. Zheng, M. Zheng, A. J. Shih, and K. Xu, "An Endoscopic Continuum Testbed for Finalizing System Characteristics of a Surgical Robot for NOTES Procedures," in *IEEE/ASME International Conference on Advanced Intelligent Mechatronics (AIM)*, Wollongong, Australia, 2013, pp. 63-70.
- [12] J. R. Romanelli and D. B. Earle, "Single-Port Laparoscopic Surgery: an Overview," *Surgical Endoscopy*, vol. 23, No.7, pp. 1419-1427, April 2009.
- [13] P. P. Rao, P. P. Rao, and S. Bhagwat, "Single-incision Laparoscopic Surgery - Current Status and Controversies," *Journal of Minimal Access Surgery*, vol. 7, No.1, pp. 6-16, 2011.
- [14] H. Lee, Y. Choi, and B.-J. Yi, "Stackable 4-BAR Manipulators for Single Port Access Surgery," *IEEE/ASME Transaction on Mechatronics*, vol. 17, No.1, pp. 157-166, Feb 2012.
- [15] M. Piccigallo, U. Scarfogliero, C. Quaglia, G. Petroni, P. Valdastrì, A. Menciassi, and P. Dario, "Design of a Novel Bimanual Robotic System for Single-Port Laparoscopy," *IEEE/ASME Transactions on Mechatronics*, vol. 15, No.6, pp. 871-878, Dec 2010.
- [16] Y. Sekiguchi, Y. Kobayashi, Y. Tomono, H. Watanabe, K. Toyoda, K. Konishi, M. Tomikawa, S. Ieiri, K. Tanoue, M. Hashizume, and M. G. Fujie, "Development of a Tool Manipulator Driven by a Flexible Shaft for Single Port Endoscopic Surgery," in *IEEE / RAS-EMBS International Conference on Biomedical Robotics and Biomechanics (BIOROB)*, Tokyo, Japan, 2010, pp. 120-125.
- [17] G.-P. Haber, M. A. White, R. Autorino, P. F. Escobar, M. D. Kroh, S. Chalikhonda, R. Khanna, S. Forest, B. Yang, F. Altunrende, R. J. Stein, and J. H. Kaouk, "Novel Robotic da Vinci Instruments for Laparoendoscopic Single-site Surgery," *Urology*, vol. 76, No.6, pp. 1279-1282, Dec 2010.
- [18] K. Xu, R. E. Goldman, J. Ding, P. K. Allen, D. L. Fowler, and N. Simaan, "System Design of an Insertable Robotic Effector Platform for Single Port Access (SPA) Surgery," in *IEEE/RSJ International Conference on Intelligent Robots and Systems (IROS)*, St. Louis, MO, USA, 2009, pp. 5546-5552.
- [19] J. Ding, R. E. Goldman, K. Xu, P. K. Allen, D. L. Fowler, and N. Simaan, "Design and Coordination Kinematics of an Insertable Robotic Effectors Platform for Single-Port Access Surgery," *IEEE/ASME Transactions on Mechatronics*, vol. 18, No.5, pp. 1612-1624, Oct 2013.
- [20] M. Simi, M. Silvestri, C. Cavallotti, M. Vatteroni, P. Valdastrì, A. Menciassi, and P. Dario, "Magnetically Activated Stereoscopic Vision System for Laparoendoscopic Single-Site Surgery," *IEEE/ASME Transactions on Mechatronics*, vol. 18, No.3, pp. 1140-1151, June 2013.
- [21] K. Xu and N. Simaan, "An Investigation of the Intrinsic Force Sensing Capabilities of Continuum Robots," *IEEE Transactions on Robotics*, vol. 24, No.3, pp. 576-587, June 2008.
- [22] K. Xu and N. Simaan, "Analytic Formulation for the Kinematics, Statics and Shape Restoration of Multibackbone Continuum Robots via Elliptic Integrals," *Journal of Mechanisms and Robotics*, vol. 2, Feb 2010.
- [23] R. J. Webster and B. A. Jones, "Design and Kinematic Modeling of Constant Curvature Continuum Robots: A Review," *International Journal of Robotics Research*, vol. 29, No.13, pp. 1661-1683, Nov 2010.
- [24] Z. Zhang, "Flexible Camera Calibration by Viewing a Plane from Unknown Orientations," in *IEEE International Conference on Computer Vision (ICCV)*, Kerkyra, 1999, pp. 666-673.
- [25] R. Y. Tsai, "A Versatile Camera Calibration Technique for High Accuracy 3D Machine Vision Metrology Using Off-the-Shelf TV Cameras and Lenses," *IEEE Journal of Robotics and Automation*, vol. 3, No.4, pp. 323-344, 1987.